Journal of Non-Crystalline Solids 534 (2020) 119884

Contents lists available at ScienceDirect

Journal of Non-Crystalline Solids

journal homepage: www.elsevier.com/locate/jnoncrysol

Structural and electrical characterization of semiconducting xCuO-(100-x)TeO_2 glasses

Navjot Kaur[a], Atul Khanna[a,*], Margit Fábián[b], Shankar Dutt[a]

[a] Department of Physics, Guru Nanak Dev University, Amritsar 143005, Punjab, India
[b] Centre for Energy Research, Konkoly-Thege street 29-33, Budapest 1121, Hungary

ARTICLE INFO

Keywords:
Semiconducting copper tellurite glasses
Neutron diffraction
Reverse Monte Carlo simulations
Structure
Laser induced crystallization
Dc conductivity and thermal properties

ABSTRACT

Structural, thermal and electrical properties of semiconducting copper tellurite glasses: xCuO-(100-x)TeO_2 (x = 30, 40 and 50 mol%) were studied by neutron diffraction, Raman spectroscopy, thermal analysis and two probe electrical conductivity measurements. Reverse Monte Carlo simulations of the neutron structure factors found that Te—O and Cu—O bonds have equal lengths of 1.94 Å and that both Te and Cu ions exist in structural units of similar size and geometry. The average Cu—O co-ordination decreases from 3.72 to 3.68, while the Te—O co-ordination decreases from 3.48 to 3.34 on increasing the CuO concentration from 30 to 50 mol%. The electrical conductivity increases from 2.96 × 10^{-9} Ω^{-1} m^{-1} to 1.25 × 10^{-7} Ω^{-1} m^{-1} with an increase in CuO concentration from 30 to 50 mol%. The increase in CuO mol% increases the Cu—Cu coordination number from 0.68 to 1.26 and promotes electronic hopping between the adjacent Cu sites.

1. Introduction

Semiconducting glasses show electrical conductivity higher than 10^{-7} Ω^{-1} m^{-1} at room temperature (298 K) and have a negative temperature coefficient of resistance [1–3]. In these glasses the electron conduction takes place due to the transport of electrons or holes. Chalcogenide glasses containing Se, Te etc. are semiconductors [4–8]. The chalcogenide glasses are generally p-type semiconductors and this can reverse to n-type conduction by doping with other atoms [5,9]. It is reported that the conductivity of $(Ag)_x(GeSe_3)_{(1-x)}$ ($0 \leq x \leq 0.571$) glasses increases from 10^{-12} Ω^{-1} m^{-1} to 10^{-1} Ω^{-1} m^{-1} at room temperature as the concentration of silver increases in the glass system [10].

Tellurite glasses are oxide glasses that have several useful properties such as high chemical stability, low melting temperatures of 873–1223 K, low phonon energies (maximum phonon energies of ~800 cm^{-1}), high dielectric constants and high transmittance in the visible to near- infrared region [11–13]. The pure TeO_2 glass is difficult to synthesize because it requires very high melt quenching rates of 10^5 K s^{-1} [14,15]. On the other hand, if TeO_2 is mixed with alkali, alkaline-earth, heavy metal and rare earth oxides the quenching rates required for glass formation decreases significantly and tellurite glasses can be prepared at moderate quenching rates of 10^2–10^3 K s^{-1} [11]. The tellurite glasses containing transition metal oxides such as CuO [16], V_2O_5 [17,18] and Fe_2O_3 [19] exhibit semiconducting behaviour and have applications in memory devices and as cathodes in secondary storage batteries [20,21]. The partially filled d-orbitals characterize transition metal (TM) ions and the latter can exist in a variety of oxidation states, this property produces semi-conducting behaviour of TM ion glasses via electron transfer from ions in a lower valence state to the ions in a higher valence state [22,23].

The electrical conductivity behaviour of TM-ion-containing tellurite glasses is generally explained by small polaron theory [16,22–25]. Ghosh reported that the conductivity of copper tellurite glasses of the composition: xCuO-(100-x)TeO_2 (x = 37.40, 47.30, 56.36 and 64.14 mol%) increases from 10^{-6} Ω^{-1} m^{-1} to 10^{-4} Ω^{-1} m^{-1} at 450 K as the concentration of CuO increases, and the activation energy of the glasses with higher CuO content is low and that the conduction in copper tellurite glasses is electronic instead of ionic [16]. Although the electrical properties of xCuO-(100-x)TeO_2 glasses have been studied earlier [16,22], their structural-property data which can contribute to the understanding and modelling of electrical conduction is not available.

X-ray diffraction [26–28] and neutron diffraction studies on the structure of tellurite glasses have revealed that these glasses predominantly consist of TeO_4 trigonal bi-pyramids, deformed TeO_4, TeO_{3+1} and TeO_3 trigonal pyramidal units [13,29,30]. The conversion of TeO_4 into TeO_3 with the addition of metal oxides is also confirmed by

* Corresponding author.
E-mail address: atul.phy@gndu.ac.in (A. Khanna).

https://doi.org/10.1016/j.jnoncrysol.2020.119884
Received 26 November 2019; Received in revised form 31 December 2019; Accepted 2 January 2020
Available online 03 March 2020

Raman studies on tellurite glasses [13,31,32]. Neutron and x-ray diffraction serve as non-invasive and direct techniques for studying the short-range and intermediate-range order in amorphous materials [33–35]. In multi-component glass system, the nearest neighbours' atomic correlations information is difficult to extract from the diffraction data due to overlapping of a large number of atomic pair correlation functions which have peaks at same distances [36]. Therefore, in order to solve this problem, Reverse Monte Carlo (RMC) technique is employed which gives partial atomic pair correlation functions and hence provide an accurate data on coordination numbers, bond lengths and bond angle distributions [37–39].

It is the objective of the present study to determine the short-range structural properties of xCuO-(100-x)TeO_2 (x = 30%, 40% and 50%) glasses and correlate the structural properties with its electrical conductivity.

2. Experimental studies

2.1. Glass preparation and density measurement

Glasses of composition: xCuO-(100-x)TeO_2 (x = 30, 40 and 50 mol %) were prepared by melt quenching by using CuO (99.9% Sigma Aldrich, India) and TeO_2 (99% Sigma Aldrich, India) as starting materials. The appropriate amount of these materials were weighed, mixed, transferred to a platinum crucible and melted at 1073 K for 1 h in a muffle furnace. The samples of batch weights of ~10 g were prepared by normal quenching method at cooling rates of $\sim 10^2$ K s^{-1}. The composition, mass-densities and atomic number densities for the samples are given in Table 1. The densities were determined by Archimedes method using dibutyl-pthalate as the immersion fluid.

2.2. X-ray diffraction

X-ray diffraction studies were carried out on Shimadzu Maxima-7000 powder X-ray diffractometer at room temperature with Cu-$K_{\alpha 1}$ radiation (λ = 1.5406 Å) in 2θ range of 10–80°. The X-ray tube was operated at 40 kV and 30 mA and the scattered intensity was measured with the scintillation detector.

2.3. Thermal properties

Thermal properties were studied by DSC on a SETARAM Setsys 16 TG-DSC system in the temperature range of 473–1050 K at a heating rate of 10 K min^{-1} in air atmosphere. The maximum uncertainty in the mid-point glass transition (T_g), peak crystallization (T_c) and peak melting temperatures (T_m) is ± 1 K and the values are given in Table 1.

2.4. Electrical properties

The direct current (DC) electrical conductivities of glasses were measured by depositing silver coating on the two sides of the disk-shaped samples and by using high temperature two probe setup (TPX-600, SES Instruments Pvt. Ltd., Roorkee, India). Voltage of 10 V was applied on the two contacts and the current was measured with a digital picoammeter (Keithley, Model 485) by varying the temperature from 303 K to 418 K. The conductivity was determined by the following formula:

$$\sigma = \frac{t}{RA} \tag{1}$$

where R is the resistance, A is the area and t is the thickness of the sample.

The activation energy for electrical conduction was calculated from the formula given by Mott [40,41]:

$$\sigma = \sigma_o \exp\left(-\frac{E_a}{kT}\right) \tag{2}$$

where σ_o pre-exponential factor and E_a is the activation energy. The slope between ln(σ) and 1000/T gives the activation energy (E_a) of samples, and its values are given in Table 2.

2.5. Neutron diffraction

Neutron diffraction studies on copper tellurite glasses were performed at room temperature and at 473 K by using monochromatic neutrons having de-Broglie wavelength (λ = 1.068 Å) on the 2-axis PSD diffractometer in Budapest Neutron Centre, Budapest, Hungary with momentum transfer (Q) range of 0.45–9.8 $Å^{-1}$. For the neutron diffraction experiments, the glass samples of 3–4 g mass were crushed into coarse powder and placed in thin-walled cylindrical vanadium can of diameter 8 mm. The diffraction data was measured for 24 h on each sample and corrected for background, multiple scattering, absorption errors and normalized with vanadium [42–44].

2.6. Reverse Monte Carlo simulations

The standard procedures were used to find the experimental neutron structure factor S(Q). The partial atomic pair correlation functions [45], bond lengths, co-ordination numbers and bond angle distributions were determined from RMC^{++} Version 1.5.1 software developed by Pusztai et al. [37,39,46,47]. The RMC method minimizes the squared difference between the experimental and the RMC simulated S(Q) from a 3-dimensional atomic configurations and atomic correlation functions [37,39]. The following formalism was used to calculate the partial pair correlation functions, $g_{ij}(r)$ and the partial structure factors, $S_{ij}(Q)$ [38,48–51]:

$$S(Q) = \sum_{i,\,j}^{k} w_{ij} S_{ij}(Q) \tag{3}$$

$$S_{ij}(Q) = 1 + \frac{4\pi\rho_o}{Q}\int_0^{r_{max}} r[g_{ij}(r) - 1]\mathrm{Sin}Qr\ dr \tag{4}$$

$$w_{ij} = \frac{c_i b_i c_j b_j \times (2 - \delta_{ij})}{\left[\sum_i^k c_i b_i\right]^2} \tag{5}$$

where δ_{ij} is the Kroneker delta function, c_i, c_j represents molar fractions of the components, b_i, b_j denotes the corresponding coherent neutron scattering amplitude and k corresponds to the total number of elements in the sample, based on the $k(k + 1)/2$ equation we have six atomic pairs. The calculated weighting factors for the atomic pairs, are given in Table 3. The RMC simulation was initiated with an initial random atomic configuration by considering a simulated box that contained 10,000 atoms of Cu, Te and O.

Table 1
Composition, mass and atomic number density and thermal properties of copper tellurite glasses.

Sample Code	Composition (mol %)		Density, d [g·cm^{-3}] ± 0.005	Molar Volume, V_m [cm^3 mol^{-1}]	Atomic number density, ρ_o [$Å^{-3}$]	T_g [K]	T_c [K]		T_m [K]		
	CuO	TeO_2					T_{c1}	T_{c2}	T_{m1}	T_{m2}	T_{m3}
30CuTe	30	70	5.634	24.06	0.06756	578	676	701	856	-	-
40CuTe	40	60	5.603	22.76	0.06876	575	691	716	893	-	-
50CuTe	50	50	5.591	21.38	0.07039	571	725	-	769	863	877

Table 2
Electrical properties of copper tellurite glasses.

Sample code	σ (Ω^{-1} m^{-1})		E_a (eV)	σ_o (Ω^{-1} m^{-1})	R (Å)	N (10^{28} m^{-3})
	303K	418K				
30CuTe	2.96×10^{-9}	2.34×10^{-6}	0.64	4.5×10^{5}	2.74	0.75
40CuTe	1.25×10^{-8}	7.05×10^{-6}	0.62	1.6×10^{6}	2.84	1.05
50CuTe	1.25×10^{-7}	4.39×10^{-5}	0.58	3.8×10^{6}	2.90	1.41

Table 3
Neutron scattering weight factors, w_{ij} (%), r_{min} and r_{max} values used to calculate coordination numbers by RMC simulations.

Atom Pair	30CuTe			40CuTe			50CuTe		
	w_{ij} (%)	r_{min}(Å)	r_{max}(Å)	w_{ij} (%)	r_{min}(Å)	r_{max}(Å)	w_{ij} (%)	r_{min}(Å)	r_{max}(Å)
Cu-Cu	2.0	2.24	3.10	3.8	2.29	3.15	6.2	2.25	3.27
Cu-Te	7.1	2.41	3.18	8.5	2.42	3.18	9.4	2.43	3.25
Cu-O	17.3	1.69	2.31	22.8	1.69	2.20	28.1	1.69	2.17
Te-Te	6.2	2.99	3.95	4.8	3.00	4.01	3.5	3.05	4.01
Te-O	30.3	1.69	2.32	25.7	1.69	2.34	21.1	1.69	2.34
O-O	36.9	2.20	3.26	34.3	2.20	3.34	31.7	2.20	3.40

The atomic densities, ρ_o were 0.06756 $Å^{-3}$, 0.06876 $Å^{-3}$ and 0.07039 $Å^{-3}$ for the samples: 30CuTe, 40CuTe and 50CuTe respectively (Table 1). The atomic pair correlation functions and coordination number distrubutions were determined by repeatedly performing RMC runs by slightly changing the interatomic cut-off distances until the RMC simulated S(Q) matched with the experimental S(Q). No co-ordination constraint was applied in the RMC simulations.

The final cut-off distances used in the RMC runs for Cu—Cu, Cu—Te, Cu—O, Te—Te, Te—O and O—O for the three copper tellurite samples were 2.30, 2.60, 1.60, 2.22, 1.60 and 2.30 Å. The coordination numbers for these samples were calculated from the r_{min} and r_{max} values that are listed in Table 3.

The atomic pair correlation distribution g(r) were calculated from the weighted sum of partial atomic pair correlations $g_{ij}(r)$, by using the following relationship [38,47] :

$$g(r) = \sum_{i,j} w_{ij} g_{ij}(r) \quad (6)$$

2.7. Raman spectroscopy

Renishaw In-Via Reflex micro-Raman spectrometer was used to measure the Raman spectra of the glasses by using an argon ion laser of 514.5 excitation wavelength, a diffraction grating having 2400 lines mm^{-1} and an edge filter for Stokes spectra and a Peltier cooled CCD detector. Measurements were performed in an unpolarized mode at room temperature in the back-scattering geometry in the wave number range of 30–1100 cm^{-1} at a spectral resolution of ~ 0.5 cm^{-1}.

3. Results and discussion

3.1. X-ray diffraction

The XRD patterns of xCuO-(100-x)TeO_2 (x = 20, 30, 40 and 50 mol %) samples are shown in Fig 1. These patterns show a broad hump without any sharp peak which confirms the amorphous nature of samples. The sample of composition: 20CuO–80TeO_2 glass was also prepared but its XRD pattern showed several sharp peaks along with the broad hump. These sharp peaks match with orthorhombic $CuTeO_3$ [PDF #75-0635], monoclinic $CuTeO_3$ [PDF #84-1482], tetragonal TeO_2 [PDF #78-1714] and orthorhombic TeO_2 [PDF #76-0680] phases that are marked by different symbols in Fig. 1, therefore this sample was not a pure glass sample but a glass-ceramic.

The glass-forming ability of xCuO-(100-x)TeO_2 system increases significantly with an increase in CuO concentration from 30 to 50 mol% and the amorphous nature of these samples is confirmed by the broad humps in the XRD patterns as shown in Fig. 1.

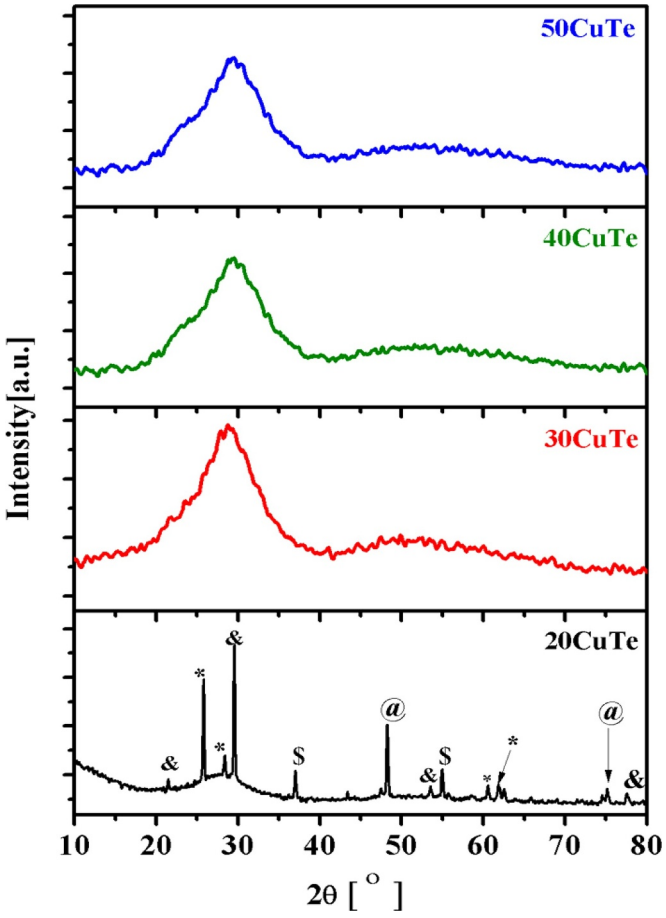

Fig 1. XRD patterns of xCuO-(100-x)TeO_2 (x = 30, 40 and 50 mol%) glasses showing their amorphous nature. Sample 20CuTe is semicrystalline with sharp peaks due to monoclinic $CuTeO_3$ (&), orthorhombic $CuTeO_3$ (*), tetragonal TeO_2 ($) and orthorhombic TeO_2 (@).

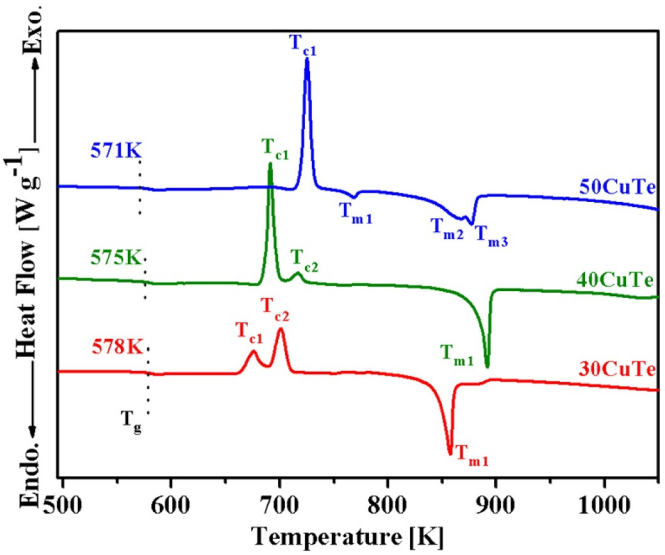

Fig 2. DSC scans of xCuO-(100-x)TeO_2 glasses. .

3.2. Density

The glass density decreases from 5.634 to 5.591 g cm^{-3} with an increase in CuO concentration from 30 to 50 mol% and is due to the replacement of heavier TeO_2 (159.6 g mol^{-1}) by the lighter CuO (79.54 g mol^{-1}) (Table 1). The molar volume, V_m also decreases from 24.06 to 21.38 cm^3 mol^{-1} due to the replacement of Te^{4+} (0.66 Å) by smaller Cu^{2+} (0.57 Å) [52] and also may be due to the increase in the concentration of non-bridging oxygens in the glass network [24]. The monotonic variation of V_m with the increase in concentration of CuO in the samples shows that the single-phase random network structure exist in the glasses [53].

3.3. Thermal properties

The DSC plots of copper tellurite glasses are shown in Fig. 2. The value of mid-point T_g (glass transition temperature) decreases from 578 K to 571 K as the concentration of CuO increases from 30 to 50 mol % due to lower bond enthalpy of Cu-O bonds (343 kJ mol^{-1}) as compared to Te—O bonds (391 kJ mol^{-1}) [54]. Also, with increase in CuO concentration, the peak corresponding to crystallization temperature reduces to a single peak. The values of the mid-point glass transition

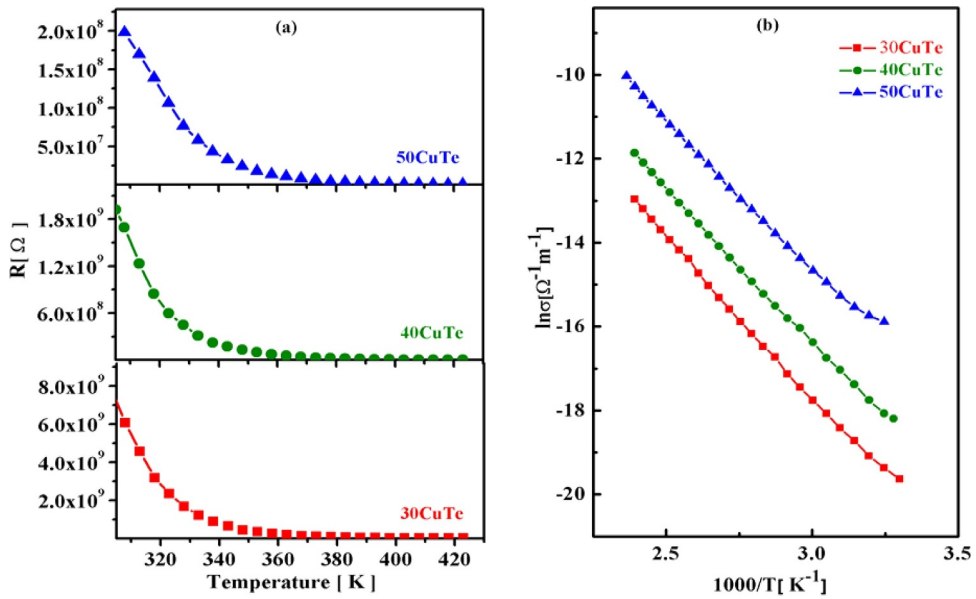

Fig 3. (a) The variation of resistance with temperature (b) Arrhenius plots of DC conductivity in xCuO-(100-x)TeO_2 glasses (c) plot of ln(σT) vs 1000/T.

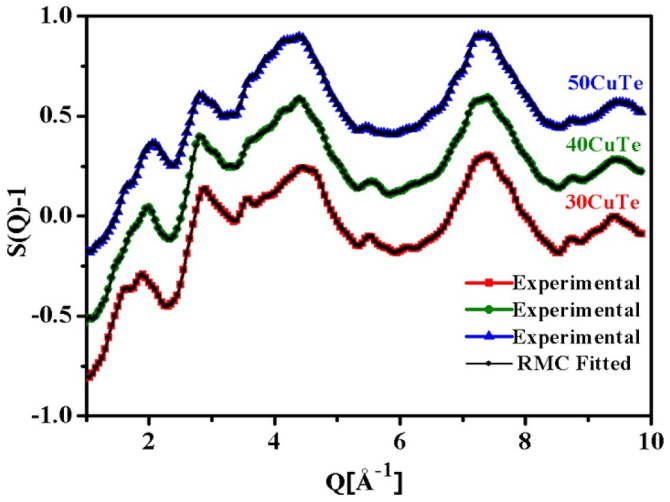

Fig 4. Experimental and RMC-calculated neutron structure factors of xCuO-(100-x)TeO_2 glasses.

temperature, T_g, crystallization temperature, T_c and melting temperature, T_m are given in Table 1.

3.4. Electrical properties

The electrical conductivity of three copper tellurite glasses increases from 2.96 × 10^{-9} to 2.34 × 10^{-6} Ω^{-1} m^{-1} (30CuTe sample), 1.25 × 10^{-8} to 7.05 × 10^{-6} Ω^{-1} m^{-1} (40CuTe sample) and 1.25 × 10^{-7} to 4.39 × 10^{-5} Ω^{-1} m^{-1} (50CuTe sample) as the temperature increases from 303 K to 418 K. It shows that with an increase in temperature, the conductivity increases which confirms the semiconducting nature of all copper tellurite glasses. The resistance versus temperature graph is displayed in Fig. 3a.

Fig. 3b shows the ln(σ) versus 1000/T graphs of copper tellurite glasses. The conductivity increases as the concentration of CuO increases from 30 to 50 mol%. The conduction process in these glasses is based on the small polaron hopping model and according to this model the conduction in glasses containing transition metal ion (Cu^+ and Cu^{2+}) occurs by thermally assisted small polaron hopping [55] from low valence state (Cu^+) to the high valence state (Cu^{2+}) of the transition metal ion. At higher temperature range ($T > \theta_D/2$), the

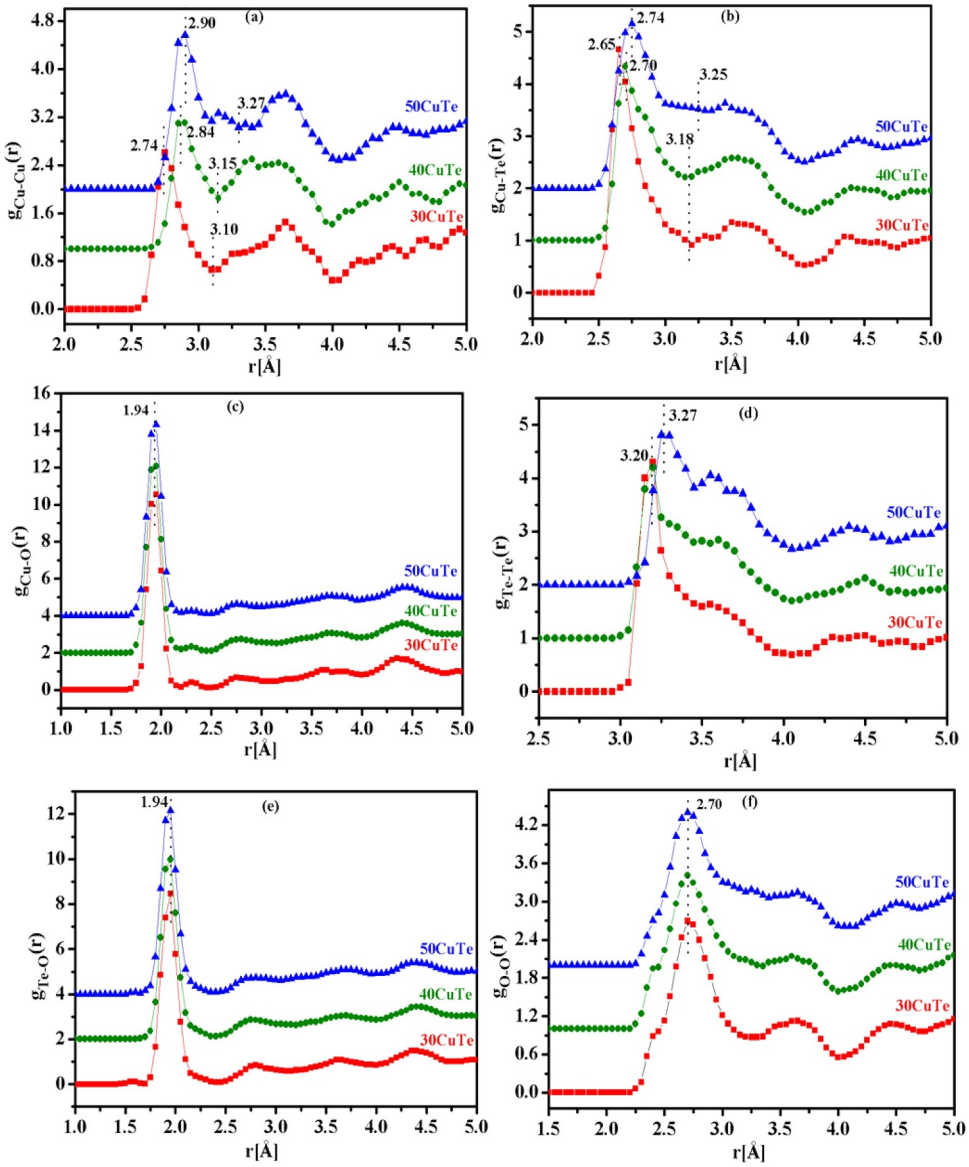

Fig 5. Partial atomic pair correlation functions for (a) Cu—Cu (b)Cu—Te (c) Cu—O (d) Te—Te (e) Te—O and (f) O—O correlations in copper tellurite glasses.

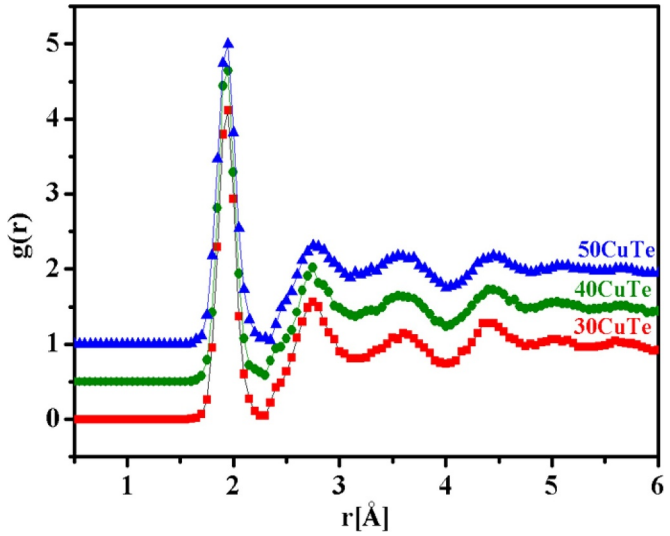

Fig. 6. Atomic pair correlation functions of three copper tellurite glasses obtained by the weighted sum of partial pair correlations.

conductivity in the non-adiabatic regime is given by [41]:

$$\sigma = \frac{\nu_0 Ne^2R^2}{kT} c(1-c) e^{-2\alpha R}\, e^{-E_a/kT} \quad (7)$$

where ν_0 is the phonon frequency, R is the average hopping spacing (Cu—Cu distances), α is the electron wave function decay constant and E_a is the activation energy, c the ratio of the concentration of TM ions in low valence state to the total number of ions, N, and θ_D is the Debye temperature. The term $e^{-2\alpha R}$ becomes unity as the polaron hopping is in the adiabatic regime for copper tellurite glasses [16,22] and the Eq. (7) becomes:

$$\sigma = \frac{\nu_0 Ne^2R^2}{kT} c(1-c)\, e^{-E_a/kT} \quad (8)$$

It is also observed that there is a break of linearity in ln(σ) versus 1000/T plots at 311 K and according to the small polaron model, this happens at $\theta_D/2$ (Fig. 3b). This is a feature of small polaron model [16,22,25]. The pre-exponential factor was calculated from the intercept of ln(σT) vs 1000/T plot (Fig. 3c). The activation energy was calculated from the slope of the graphs and it decreases from 0.64 eV to 0.58 eV as CuO concentration increases from 30 to 50 mol%. The values of σ and E_a are presented in Table 2.

3.5. Short-range structure by neutron diffraction and RMC simulations

The experimental and RMC calculated S(Q) of three copper tellurite glasses matched perfectly as shown in Fig. 4. The partial atomic pair correlation functions i.e. $g_{Cu\text{-}Cu}$, $g_{Cu\text{-}Te}$, $g_{Cu\text{-}O}$, $g_{Te\text{-}Te}$, $g_{Te\text{-}O}$ and g_{O-O} were determined from RMC simulation and are shown in Fig. 5a–f. The first peaks of $g_{Cu\text{-}O}$ and $g_{Te\text{-}O}$ exist at the same distance of 1.94 ± 0.02 Å and that of g_{O-O} is at 2.70 ± 0.05 Å in the glass samples; 30CuTe, 40CuTe and 50CuTe. Within the limits of experimental uncertainties the Te—O, Cu—O and O—O nearest neighbour distances do not show any changes with an increase in CuO mol%. The atomic pair correlation functions, g(r) of three copper tellurite glasses were obtained by the weighted sum of partial atomic pair correlations and are shown in Fig. 6. The bar graphs in Fig. 7a-c give the distribution of Te—O, Cu—O

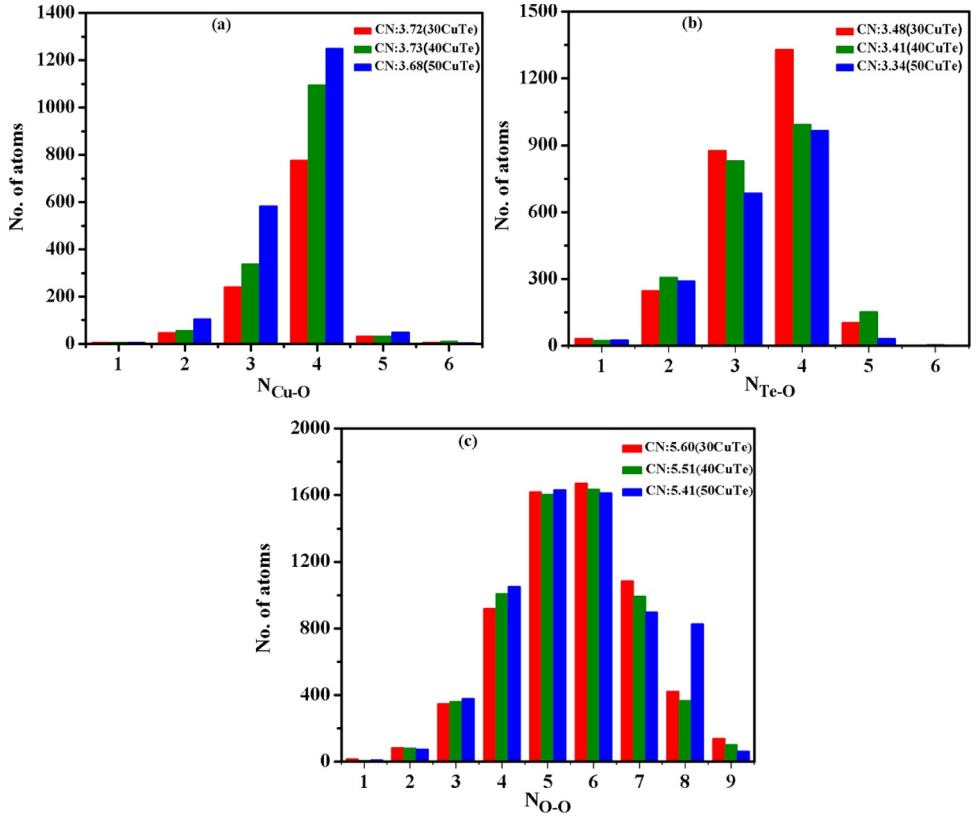

Fig 7. Coordination number distributions of (a) Cu—O (b) Te—O (c) O—O correlations in glasses.

Table 4
Structural properties of copper tellurite glasses from RMC simulations and Raman spectroscopy.

		30CuTe	40CuTe	50CuTe
Nearest neighbour distance, r_{ij}[Å]	Cu-Cu	2.74 ± 0.05	2.84 ± 0.05	2.90 ± 0.05
	Cu-Te	2.65 ± 0.10	2.70 ± 0.10	2.74 ± 0.10
	Cu-O	1.94 ± 0.02	1.94 ± 0.02	1.94 ± 0.02
	Te-Te	3.20 ± 0.10	3.20 ± 0.10	3.27 ± 0.10
	Te-O	1.94 ± 0.02	1.94 ± 0.02	1.94 ± 0.02
	O-O	2.70 ± 0.05	2.70 ± 0.05	2.70 ± 0.05
Coordination number, CN_{ij}	Cu-O	3.72 ± 0.03	3.73 ± 0.03	3.68 ± 0.03
	$Te\text{-}O_{(neutron)}$	3.48 ± 0.03	3.41 ± 0.03	3.34 ± 0.03
	$Te\text{-}O_{(Raman)}$	3.48 ± 0.02	3.43 ± 0.02	3.39 ± 0.02
	O-O	5.60 ± 0.05	5.51 ± 0.05	5.41 ± 0.05
	Cu-Cu	0.68 ± 0.05	0.82 ± 0.05	1.26 ± 0.05
	Cu-Te	0.62 ± 0.05	0.84 ± 0.05	1.41 ± 0.05
Bond angle θ_{ij} [°]	O-Cu-O	88 ± 1	88 ± 1	88 ± 1
	O-Te-O	88 ± 2	88 ± 2	88 ± 2
	O-O-O	60 ± 2	60 ± 2	60 ± 2
	Cu-O-Cu	92 ± 3	97 ± 3	97 ± 3
	Te-O-Te	115 ± 3	109 ± 3	111 ± 3

and O—O co-ordinations in the copper tellurite glasses.

RMC simulations found that the coordination number of Te with oxygens decreases steadily from 3.48 ± 0.02 to 3.34 ± 0.02 as the concentration of CuO increases from 30 to 50 mol% and this is due to the structural transformations: $TeO_4 \rightarrow TeO_{3+1} \rightarrow TeO_3$ [20], the latter transformation causes depolymerisation or breakage of the Te—O network. The co-ordination of Cu—O is 3.72 ± 0.03 in 30CuTe, 3.73 ± 0.03 in 40CuTe and 3.68 ± 0.03 in 50CuTe (Table 4) which confirms that copper ions are mostly tetrahedrally coordinated with oxygens due to Jahn-Teller distortion [56]. Further both Cu—O and Te—O coordinations reduce by small but significant amounts with increase in CuO content. The Cu—Cu coordination number increases from 0.68 ± 0.05 to 1.26 ± 0.05 as the concentration of CuO increases from 30 to 50 mol% and this promotes the hopping electronic conduction.

The bond angle of Cu—O—Cu linkages increases from 92 ± 3° to 97 ± 3° as the concentration of CuO increases from 30 to 50 mol% (Fig. 8a). The bond angle distributions of O—Cu—O have peaks at 88 ± 1°, O—Te—O at 88 ± 2°, Te—O—Te in the range: 109–115° ± 3° and O—O—O at 60 ± 2° (Fig. 8b, c, d and –e). It is known that the bond angle distribution of O—Te—O linkages in the range of 150 – 170° are

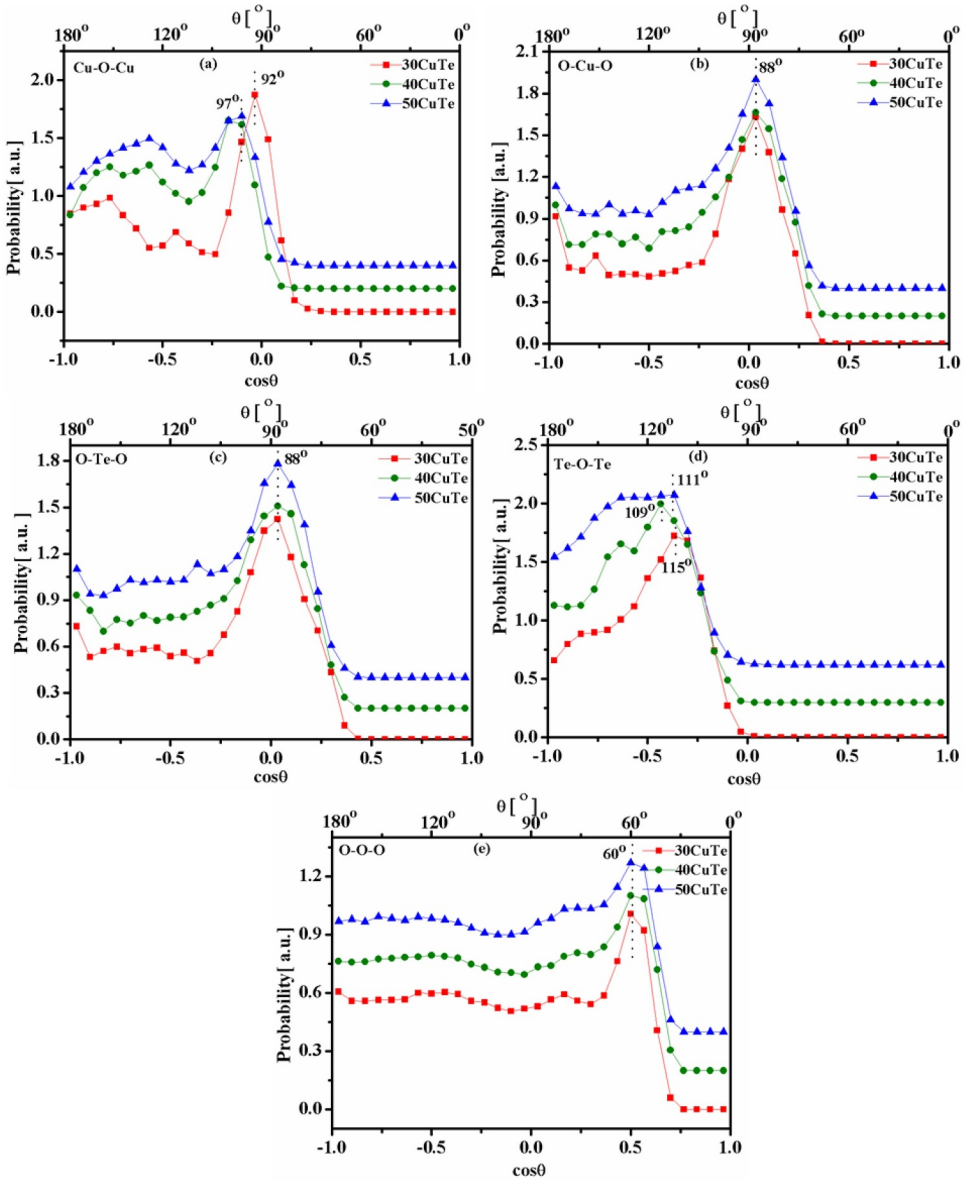

Fig. 8. Bond angle distributions for (a) Cu—O—Cu (b) O—Cu—O (c) O—Te—O (d) Te—O—Te and (e) O—O—O linkages in copper tellurite glasses.

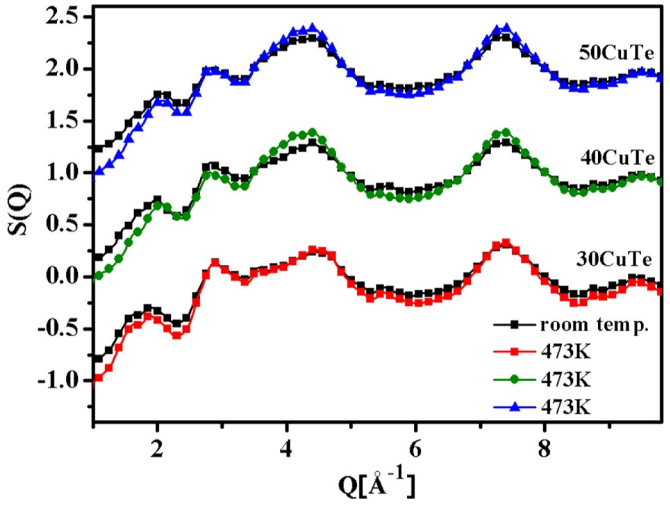

Fig. 9. Comparison of neutron structure factors at room temperature and at 473 K for xCuO-(100-x)TeO_2 glasses. Curves for different samples have been arbitrarily shifted.

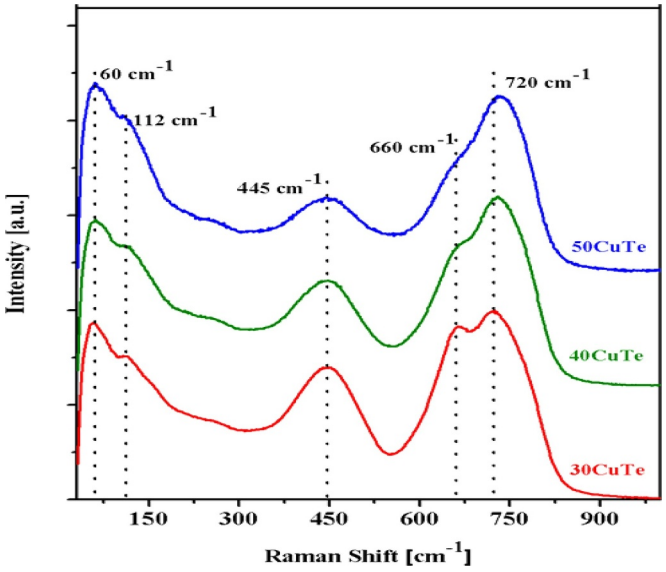

Fig 10. Raman spectra of copper tellurite glasses.

due to O_{ax}–Te–O_{ax} bonds while the peak in the lower angular range: 70 − 105° are due to O_{eq}–Te–O_{eq} and O_{eq}–Te–O_{ax} bonds [46]. In the three copper tellurite glasses, bond angle distribution of O–Te–O linkages have maxima at 88 ± 2° with little or no peak in the higher angle range: 150 − 170°, therefore O_{eq}–Te–O_{eq} and O_{eq}–Te–O_{ax} bonds are dominant in the glass network.

Insitu high temperature neutron diffraction experiments were carried out at 473 K for three copper tellurite glasses. The neutron structure factor at 473 K was the same as that at the room temperature for each sample (Fig. 9) and hence there does not occur any significant modification in the glass structure upon heating to 473 K.

3.6. Te—O speciation by Raman spectroscopy

The Raman spectra of copper tellurite glasses are shown in Fig. 10. These spectra show one strong peak at 60 cm^{-1} which is the boson peak and it is the characteristic feature of glasses [57–59]. The band at 112 cm^{-1} is due to Te—O vibrations in TeO_3 (trigonal pyramidal) units consisting of two or three non-bridging oxygens [60]. The spectra show two distinctive Raman bands in the wave number ranges: 320–554 cm^{-1} and 554–900 cm^{-1}. The Raman band at 320–554 cm^{-1} is due to bending vibrations of Te—O—Te linkages and the band at 554–900 cm^{-1} is due to asymmetric stretching vibrations of O—Te—O linkages in TeO_4 (trigonal bi-pyramidal) units and TeO_3 (trigonal pyramidal) units. The intensity of the low frequency band at 112 cm^{-1} increases, while the intensity of medium frequency band at 445 cm^{-1} reduces as the concentration of CuO increases from 30 to 50 mol% and this is due to the slow degradation of tellurite network with incorporation of CuO in the structure [61]. The intensity of the peak at 660 cm^{-1} decreases with increase in the concentration of CuO from 30 to 50 mol% and it reduces to a shoulder at 50 mol% of CuO whereas the peak at 720 cm^{-1} shifts towards a higher frequency at 736 cm^{-1}. From these changes in the Raman spectra, it is concluded that with increase in CuO mol%, the concentration of TeO_{3+1}, TeO_3 and TeO_3^{2-} unit increases and this is due to the structural transformation: $TeO_4 \rightarrow TeO_3$.

The Te—O coordination number, $N_{Te\text{-}O}$ can also be estimated from Raman studies by using the following formula [12,13,15,30,32]:

$$N_{Te-O} = 3 + \frac{I_{TeO_4}}{I_{TeO_4} + I_{TeO_3}} \quad (9)$$

where I represents the intensities of the Raman peaks. The Te—O coordination as determined from the Raman spectra of 30CuTe, 40CuTeO and 50CuTeO glasses are 3.48 ± 0.02, 3.43 ± 0.02 and 3.39 ± 0.02 respectively. It was found that the Te—O coordination decreases steadily as the concentration of CuO increases and this result is consistent with the RMC findings (Table 4).

3.7. Laser-induced crystallization

Raman spectra were measured for the samples by varying the intensity of the exciting laser (514.5 nm Argon-ion laser, maximum power = 25 mW). From these studies, it was observed that at high incident laser power, the crystallization and phase separation in three copper tellurite glasses occurs and preciptates of α-TeO_2 crystallites are produced in the glass matrix (Fig. 11) when the temperature of laser irradiated regions becomes higher than the glass transition or the crystallization temperature [62,63]. Therfore this property can be used for deliberately growing and patterning α-TeO_2 micro/ nano-crystals in the glass matrix for non-linear optical applications.

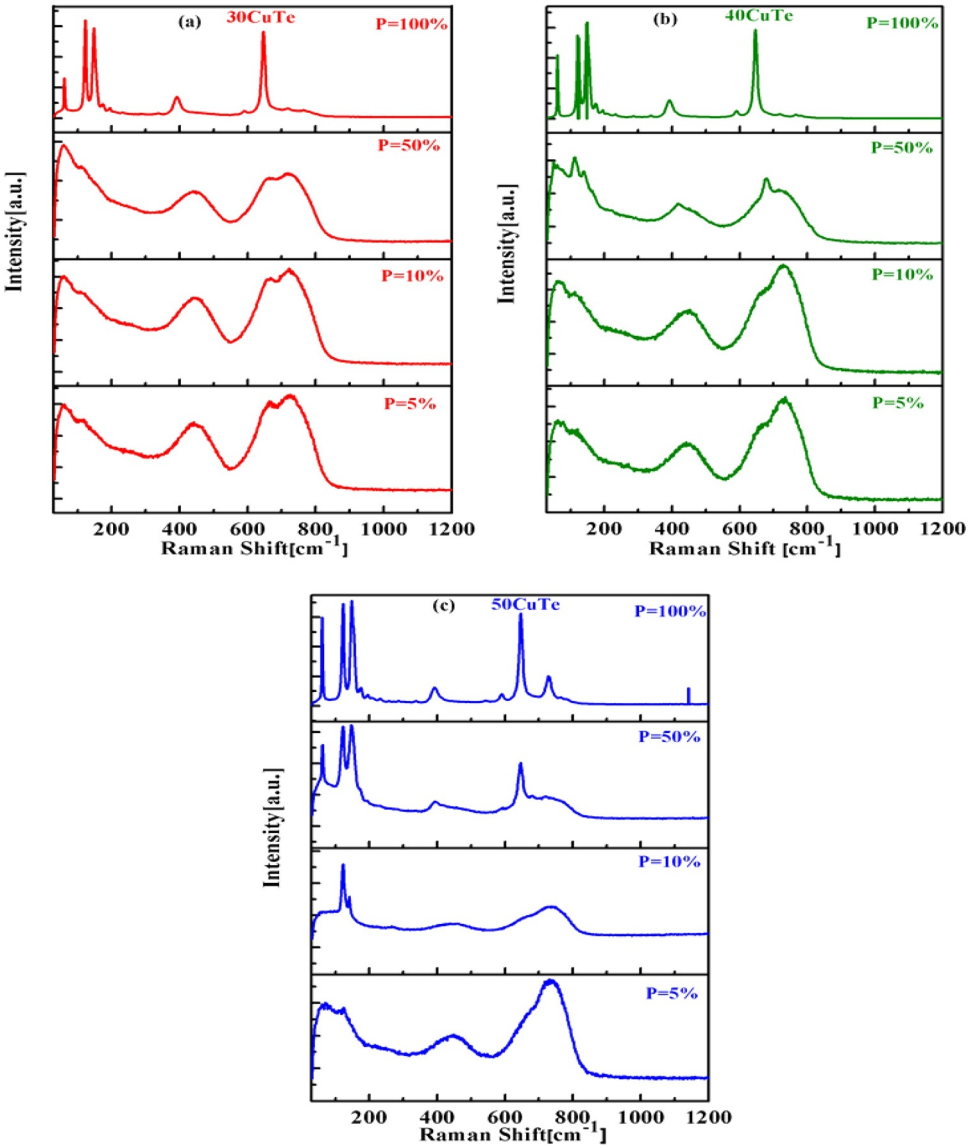

Fig 11. Raman spectra of copper tellurite glasses at different powers of the excitation laser (a) 30CuTe (b) 40CuTe and (c) 50CuTe ("P" represents power% of the excitation laser).

4. Conclusions

xCuO-(100-x)TeO_2 (x = 20, 30, 40 and 50 mol%) samples were prepared by melt quenching. The glass-forming ability of the system enhances significantly with an increase in CuO concentration from 20 to 30 mol% and purely glassy phase samples were prepared at CuO concentration of 30 mol% and more. RMC analysis found that both Te—O and Cu—O bonds have equal lengths of 1.94 Å and that Cu and Te ions exist in structural units of very similar size and geometry. Neutron diffraction studies on copper tellurite glasses were carried out at room temperature and at 473 K, and no significant changes were found in the glass short-range and medium-range order with the variation of temperature. The electrical conductivity of glasses increases steadily with increase in CuO concentration and the structural investigation concluded that this increase in the conductivity is not due to decrease in Cu–Cu separation, which on the contrary increases, but rather due to an increase in the number of nearest Cu–Cu neighbours that promotes the hopping of electrons between the adjacent copper ion sites. Finally, the laser-Raman studies have shown that these glasses can be used for patterning of α-TeO_2 crystals in the glass matrix.

CRediT authorship contribution statement

Navjot Kaur: Methodology, Writing - original draft. **Atul Khanna:** Conceptualization, Data curation, Project administration, Resources, Writing - review & editing. **Margit Fábián:** Data curation, Project administration, Resources, Writing - review & editing. **Shankar Dutt:** Methodology.

Declaration of Competing Interest

None.

Acknowledgements

Atul Khanna thanks UGC-DAE-Consotrium for Scientific Research, Mumbai and Indore Centres, Science and Engineering Research Board, Department of Science and Technology (DST), New Delhi, India for research grants.

Atul Khanna, Margit Fábián and Navjot Kaur acknowledge Indo-Hungary intergovernmental collaborative research project funded by

DST (grant no. DST/INT/HUN/P-13/2017), India and National Research Development and Innovation Office, Hungary.

References

[1] B.V. Janakirama Rao, Structure and mechanism of conduction of semiconductor glasses, J. Am. Ceram. Soc. 48 (1965) 311–319.
[2] D. Adler, Semiconducting glasses, J. Non Cryst. Solids 73 (1985) 205–214.
[3] B. Punit, Insulating and Semiconducting Glasses, World Scientific, 2000.
[4] A. Owen, Semiconducting glasses part 1: glass as an electronic conductor, Contemp. Phys. 11 (1970) 227–255.
[5] A. Wallace, A. Owen, J. Robertson, Electrical contact properties of semiconducting chalcogenide glasses, Philos. Mag. B 38 (1978) 57–70.
[6] S. Elliott, A theory of ac conduction in chalcogenide glasses, Philos. Mag. 36 (1977) 1291–1304.
[7] P.K. Singh, D. Dwivedi, Chalcogenide glass: fabrication techniques, properties and applications, Ferroelectrics 520 (2017) 256–273.
[8] A. Zakery, S. Elliott, Optical properties and applications of chalcogenide glasses: a review, J. Non Cryst. Solids 330 (2003) 1–12.
[9] N. Tohge, T. Minami, Y. Yamamoto, M. Tanaka, Electrical and optical properties of n-type semiconducting chalcogenide glasses in the system Ge–Bi–Se, J. Appl. Phys. 51 (1980) 1048–1053.
[10] M. Kawasaki, J. Kawamura, Y. Nakamura, M. Aniya, Ionic conductivity of $Ag_x(GeSe_3)_{1-x}$ ($0 \leq x \leq 0.571$) glasses, Solid State Ion. 123 (1999) 259–269.
[11] R.A. El-Mallawany, Tellurite Glasses Handbook: Physical Properties and Data, CRC press, 2016.
[12] A. Kaur, A. Khanna, F. González, C. Pesquera, B. Chen, Structural, optical, dielectric and thermal properties of molybdenum tellurite and borotellurite glasses, J. Non Cryst. Solids 444 (2016) 1–10.
[13] N. Gupta, A. Kaur, A. Khanna, F. Gonzàlez, C. Pesquera, R. Iordanova, B. Chen, Structure-property correlations in TiO_2–Bi_2O_3–B_2O_3–TeO_2 glasses, J. Non Cryst. Solids 470 (2017) 168–177.
[14] E.R. Barney, A.C. Hannon, D. Holland, N. Umesaki, M. Tatsumisago, R.G. Orman, S. Feller, Terminal oxygens in amorphous TeO_2, J. Phys. Chem. Lett. 4 (2013) 2312–2316.
[15] A. Kaur, A. Khanna, V.G. Sathe, F. Gonzalez, B. Ortiz, Optical, thermal, and str, uctural properties of Nb_2O5–TeO_2 and WO_3–TeO_2 glasses, Phase Transit. 86 (2013) 598–619.
[16] A. Ghosh, Electrical properties of semiconducting amorphous copper-tellurite glasses, J. Phys. 1 (1989) 7819.
[17] A.A. El-Moneim, DTA and IR absorption spectra of vanadium tellurite glasses, Mater. Chem. Phys. 73 (2002) 318–322.
[18] J. Kjeldsen, A.C. Rodrigues, S. Mossin, Y. Yue, Critical V_2O5/TeO_2 ratio inducing abrupt property changes in vanadium tellurite glasses, J. Phys. Chem. B 118 (2014) 14942–14948.
[19] L. Murawski, Electrical conductivity in iron-containing oxide glasses, J. Mater. Sci. 17 (1982) 2155–2163.
[20] Y. Zhang, P. Wang, T. Zheng, D. Li, G. Li, Y. Yue, Enhancing Li-Ion battery anode performances via disorder/order engineering, Nano Energy 49 (2018) 596–602.
[21] N. Krins, A. Rulmont, J. Grandjean, B. Gilbert, L. Lepot, R. Cloots, B. Vertruyen, Structural and electrical properties of tellurovanadate glasses containing Li_2O, Solid State Ion. 177 (2006) 3147–3150.
[22] P.S. Rani, R. Singh, Electrical and magnetic properties of copper tellurite glasses, J. Mater. Sci. 45 (2010) 2868–2873.
[23] I. Yahia, Y. Saddeek, G. Sakr, W. Knoff, T. Story, N. Romčević, W. Dobrowolski, Spectroscopic analysis and magnetic susceptibility of CuO–TeO_2–V_2O_5 glasses, J. Magn. Magn. Mater. 321 (2009) 4039–4044.
[24] S. Nadia, H.A. Afifi, Structure and ultrasonic properties of vanadium tellurite glasses containing copper oxide, Arch. Acoust. 34 (2009) 641–654.
[25] A. Ghosh, Electrical transport properties of molybdenum tellurite glassy semiconductors, Philos. Mag. B 61 (1990) 87–96.
[26] C. Benmore, A review of high-energy X-ray diffraction from glasses and liquids, ISRN Mater. Sci. 2012 (2012).
[27] U. Hoppe, G. Walter, G. Carl, J. Neuefeind, A. Hannon, Structure of zinc phosphate glasses probed by neutron and X-ray diffraction of high resolving power and by reverse Monte Carlo simulations, J. Non Cryst. Solids 351 (2005) 1020–1031.
[28] H. Ohno, S. Kohara, N. Umesaki, K. Suzuya, High-energy X-ray diffraction studies of non-crystalline materials, J. Non Cryst. Solids 293 (2001) 125–135.
[29] A. Gulenko, O. Masson, A. Berghout, D. Hamani, P. Thomas, Atomistic simulations of TeO_2-based glasses: interatomic potentials and molecular dynamics, Phys. Chem. Chem. Phys. 16 (2014) 14150–14160.
[30] A. Kaur, A. Khanna, M. González-Barriuso, F. González, B. Chen, Short-range structure and thermal properties of alumino-tellurite glasses, J. Non Cryst. Solids 470 (2017) 14–18.
[31] N. Gupta, A. Khanna, Glass and anti-glass phase co-existence and structural transitions in bismuth tellurite and bismuth niobium tellurite systems, J. Non Cryst. Solids 481 (2018) 594–603.
[32] A. Kaur, A. Khanna, M. Fábián, Short-range structure of barium tellurite glasses and its correlation with stress-optic response, Mater. Res. Express 5 (2018) 065203.
[33] U. Hoppe, E. Yousef, C. Rüssel, J. Neuefeind, A. Hannon, Structure of zinc and niobium tellurite glasses by neutron and x-ray diffraction, J. Phys. 16 (2004) 1645.
[34] J. McLaughlin, S. Tagg, J. Zwanziger, D. Haeffner, S. Shastri, The structure of tellurite glass: a combined NMR, neutron diffraction, and X-ray diffraction study, J. Non Cryst. Solids 274 (2000) 1–8.
[35] U. Hoppe, E. Yousef, C. Rüssel, J. Neuefeind, A. Hannon, Structure of vanadium tellurite glasses studied by neutron and X-ray diffraction, Solid State Commun. 123 (2002) 273–278.
[36] M. Fábián, E. Sváb, G. Mészáros, Z. Révay, T. Proffen, E. Veress, Network structure of multi-component sodium borosilicate glasses by neutron diffraction, J. Non Cryst. Solids 353 (2007) 2084–2089.
[37] R. McGreevy, L. Pusztai, Reverse Monte Carlo simulation: a new technique for the determination of disordered structures, Mol. Simul. 1 (1988) 359–367.
[38] M. Fábián, C. Araczki, Basic network structure of SiO_2–B_2O_3–Na_2O glasses from diffraction and reverse Monte Carlo simulation, Phys. Scr. 91 (2016) 054004.
[39] A. Kaur, A. Khanna, M. Fábián, P. Krishna, A. Shinde, Structure of lead tellurite glasses and its relationship with stress-optic properties, Mater. Res. Bull. 110 (2019) 239–246.
[40] I. Austin, N.F. Mott, Polarons in crystalline and non-crystalline materials, Adv. Phys. 18 (1969) 41–102.
[41] N. Mott, Electrons in disordered structures, Adv. Phys. 16 (1967) 49–144.
[42] A.K. Soper, P. Egelstaff, Multiple scattering and attenuation of neutrons in concentric cylinders: I. Isotropic first scattering, Nucl. Instrum. Methods 178 (1980) 415–425.
[43] N.R. Rao, P. Krishna, S. Basu, B. Dasannacharya, K. Sangunni, E. Gopal, Structural correlations in Ge_xSe_{1-x} glasses – a neutron diffraction study, J. Non Cryst. Solids 240 (1998) 221–231.
[44] Y. Waseda, The structure of non-crystalline materials, Liquids Amorph. Solids (1980).
[45] O. Gereben, P. Jóvári, L. Temleitner, L. Pusztai, A new version of the RMC++ Reverse Monte Carlo programme, aimed at investigating the structure of covalent glasses, J. Optoelectron. Adv. Mater. 9 (2007) 3021–3027.
[46] A. Khanna, M. Fábián, P.K. Hirdesh, C.J. Benmore, A. Kaur, A. Kaur, A. Shinde, P. Rajput, S. Jha, Structural analysis of WO_3–TeO_2 glasses by neutron, high energy X-ray diffraction, Reverse Monte Carlo simulations and Xanes, J. Non Cryst. Solids 495 (2018) 27–34.
[47] M. Fábián, E. Sváb, T. Proffen, E. Veress, Neutron diffraction and reverse Monte Carlo modelling of v-B_2O_3 and $75B_2O_3$–$25Na_2O$ glasses, J. Non Cryst. Solids 356 (2010) 441–446.
[48] M. Fabian, E. Svab, K. Krezhov, Network structure with mixed bond-angle linkages in MoO_3–ZnO–B_2O_3 glasses: neutron diffraction and reverse Monte Carlo modelling, J. Non Cryst. Solids 433 (2016) 6–13.
[49] H.E. Fischer, A.C. Barnes, P.S. Salmon, Neutron and x-ray diffraction studies of liquids and glasses, Rep. Prog. Phys. 69 (2005) 233.
[50] I. Kaban, P. Jóvári, W. Hoyer, E. Welter, Determination of partial pair distribution functions in amorphous $Ge_{15}Te85$ by simultaneous RMC simulation of diffraction and Exafs data, J. Non Cryst. Solids 353 (2007) 2474–2478.
[51] M. Fábián, E. Sváb, T. Proffen, E. Veress, Structure study of multi-component borosilicate glasses from high-Q neutron diffraction measurement and RMC modeling, J. Non Cryst. Solids 354 (2008) 3299–3307.
[52] J.A. Dean, Lange's Handbook of Chemistry, McGraw-Hill, Inc., New york; London, 1999.
[53] S. Sen, A. Ghosh, Structural properties of strontium vanadate glasses, J. Mater. Res. 15 (4) (2000) 995–999.
[54] T. Cottrell, The strengths of chemical bonds, 2nd edn, butterwoth, london, 1958 search pubmed;(b) B. deB. darwent, national standard reference data series, national bureau of standards, no. 31, washington, 1970 search pubmed;(c) sw benson, J. Chem. Educ. 42 (1965) 502.
[55] J.T. Devreese, Polarons, Encycl. Appl. Phys. 14 (1996) 383–409.
[56] M.A. Halcrow, Jahn–Teller distortions in transition metal compounds, and their importance in functional molecular and inorganic materials, Chem. Soc. Rev. 42 (2013) 1784–1795.
[57] A.G. Kalampounias, Low-frequency Raman scattering in alkali tellurite glasses, Bull. Mater. Sci. 31 (2008) 781–785.
[58] J. Schroeder, W. Wu, J.L. Apkarian, M. Lee, L.-G. Hwa, C.T. Moynihan, Raman scattering and Boson peaks in glasses: temperature and pressure effects, J. Non Cryst. Solids 349 (2004) 88–97.
[59] V. Malinovsky, A. Sokolov, The nature of boson peak in Raman scattering in glasses, Solid State Commun. 57 (1986) 757–761.
[60] G.W. Brady, Structure of tellurium oxide glass, J. Chem. Phys. 27 (1) (1957) 300–303.
[61] A.G. Kalampounias, Raman scattering study on vibrational modes and structure of lanthanum tellurite glasses, Chin. J. Chem. Phys. 25 (5) (2012) 519.
[62] S. Kawasaki, T. Honma, Y. Benino, T. Fujiwara, R. Sato, T. Komatsu, Writing of crystal-dots and lines by YAG laser irradiation and their morphologies in samarium tellurite glasses, J. Non Cryst. Solids 325 (2003) 61–69.
[63] T. Komatsu, R. Ihara, T. Honma, Y. Benino, R. Sato, H. Kim, T. Fujiwara, Patterning of non-linear optical crystals in glass by laser-induced crystallization, J. Am. Ceram. Soc. 90 (2007) 699–705.